Article

Short-Term Forecasting of Coastal Surface Currents Using High Frequency Radar Data and Artificial Neural Networks

Lei Ren [1,2,3] , **Zhan Hu** [2,3,4,*] **and Michael Hartnett** [5]

[1] School of Marine Engineering and Technology, Sun Yat-sen University, Guangzhou 510006, China; renleicomeon@gmail.com

[2] State-province Joint Engineering Laboratory of Estuarine Hydraulic Technology, Sun Yat-sen University, Guangzhou 510275, China

[3] Guangdong Province Engineering Research Center for Coasts, Islands and Reefs, Sun Yat-sen University, Guangzhou 510275, China

[4] School of Marine Science, Sun Yat-sen University, Guangzhou 510006, China

[5] College of Engineering and Informatics, National University of Ireland Galway, Galway H91 TK33, Ireland; michael.hartnett@nuigalway.ie

[*] Correspondence: huzh9@mail.sysu.edu.cn; Tel.: +86-020-8411-1438

check for updates

Abstract: Accurate and timely information of surface currents is crucial for various operations such as search and rescue, marine renewable energy extraction and oil spill treatment. Conventional approaches to study coastal surface currents are numerical models and observation platforms such as radars and satellites. However, both have limits. To efficiently obtain high accuracy short-term forecasting states of oceanic parameters of interest, a robust soft computing approach—Artificial Neural Networks (ANN)—was applied to predict surface currents in a tide- and wind-dominated coastal area. Hourly observed surface currents from a Coastal Ocean Dynamic Application Radar (CODAR) system, and tide and wind data from forecasting models were used to establish ANN models for Galway Bay area. One of the fastest algorithms, resilient back propagation, was used to adapt all weights and biases. This study focused on investigating the sensitivity of an ANN model to a series of different input datasets. Results indicate that correlation between ANN forecasts and observation was greater than 0.9 for both surface velocity components with one-hour lead time. Strong correlation ($\geq$0.75) was obtained between predicted results and radar data for both surface velocity components with three-hour lead time at best. However, forecasting accuracy deteriorated rapidly with longer lead time. By comparison with previous data assimilation models, in this research, best performance was achieved from ANN model's peak times of the tidally dominant surface velocity component. The forecasts presented in this research show clear improvements over previous attempts at short-term forecasting of wind- and tide-dominated currents using ANN.

Keywords: surface currents; High Frequency; radars; Artificial Neural Networks; forecasts; soft computing; CODAR

1. Introduction

Interactions between processes such as wind, surface water and tide are dominant factors driving the movement of water in coastal regions. Good understanding of surface currents is necessary for operations such as search and rescue and oil spill movement, especially short-term real time forecasting information of surface currents with high accuracy.

Numerical models and observation platforms based on remote sensing technologies are conventional tools to study characteristics of coastal surface currents and provide useful information. However, each approach has its own limits. Numerical models that mathematically describe dynamic processes are often used to produce forecasts of surface currents. Difficulties in the definition of initial and boundary conditions, grid structure on horizontal and vertical planes and simplification of parameters inevitably result in model errors that may be significant. Oceanic observation tools such as satellites, radars and Acoustic Doppler Current Profiles (ADCP) are powerful means of monitoring near real-time oceanic currents over large spatial domains; however, these tools cannot implicitly provide forecasting states of surface currents.

To obtain high accuracy forecasting states of oceanic parameters such as surface velocities by making the best use of available observations, Kalman filters, variational data assimilation and particle filters have been used as to improve modeling forecast accuracy [1–4]. However, the establishment of a data assimilation system is a major task as it usually requires significant computational cost such as the calculation of model background errors in Kalman filters and the adjoint model in four-dimensional variational (4D-VAR) data assimilation systems [5]. Other forecasting techniques include Decision Tree (DT), Fuzzy Inference System (FIS) and Artificial Neural Networks (ANN) using observations of coastal parameters [6–8]. Soft computing approaches can be generally categorized into one of two types based on the learning algorithm: (i) supervised soft computing approaches such as ANN and DT; and (ii) unsupervised soft computing approaches such as Principal Component Analysis (PCA), clustering algorithms and self-organizing maps (SOM). A supervised soft computing model is developed herein via training processes that not only generate forecasts but also correct forecasts when they deviate significantly from the target outputs in the training dataset. Training procedures are run until forecasts reach a desired level of accuracy on the training dataset. In unsupervised soft computing approaches, models are built up by reducing data structures, such as dimensionality. System reduction of redundancy via a mathematical process or organization of data by similarity may be used for unsupervised soft computing approaches [9–11]. For example, PCA is a statistical unsupervised procedure that uses an orthogonal transformation to convert a dataset of possibly correlated variables into a set of values of linearly uncorrelated principal components [12].

Since relationships between input and output variables are directly correlated in soft computing approaches, the development process is less time-consuming and faster than conventional fluid dynamics models. Because the authors focused on predicting coastal surface velocities in terms of observed surface currents in this research, a supervised soft computing approach, ANN, was adopted in this research to develop an accurate short-term forecasting system. Several researchers have successfully applied ANN algorithms in various fields to produce forecasts of diverse parameters: Chen and Lin [13] applied ANN to predict mobile station location; Aydogan et al. [14] employed ANN to predict current velocity in the Strait of Istanbul using ADCP data; Partal et al. [15] developed daily precipitation forecasts model with ANN; Makarynskyy et al. [16] applied ANN to predict waves at the west coast of Portugal; Yang and Xia [17] developed data-driven forecasting model of mining subsidence based on field measurements and artificial neural networks; and Erzin and Cetin [18] applied ANN to predict the critical factor of safety of homogeneous finite slopes. Zabada and Shahrour [19] analyzed heating expenses in a large social housing stock in the north of France using ANN model. All the studies showed that ANN algorithms are powerful and efficient for extracting internal relationships among input, and can generate high accuracy forecasting states in a wide range of application. Additionally, a wide range of ocean, coastal and environmental issues have already been solved using ANNs to approximate nonlinear processes without any knowledge of interrelations among the variables [20–23]. In this research, the authors focused on using high frequency radar (HFR) data to develop ANN forecast models through examining historical observation as input variables and optimizing topology of input variables to extend practical forecasting period for ocean surface currents. The advantages of using ANN algorithms over other techniques are:

(1)   ANN is a highly nonlinear algorithm, capable of describing nonlinear dynamic processes such as surface currents generated by tide and winds of interest here.

(2)   ANN algorithms provide the capability of dealing with datasets in the absence of knowledge about system physics.

(3)   ANN techniques use meshless computational approaches to directly correlate relationships between input variables and output variables through recognizing historic patterns [24].

(4)   ANN models require much less computational cost than conventional fluid dynamics models.

(5)   Once an ANN model is established and validated, it can be used for other periods of interest as long as appropriate input datasets are available.

(6)   ANN models are capable of dealing with finite number of discontinuities [25].

(7)   ANN models are suitable for parallel processing if long term or fast outputs are required [25].

The primary objective of this research was to assess the potential for applying ANN algorithms to develop high-accuracy forecasts of surface currents using HFR data recorded at Galway Bay. Products of short-term high accuracy surface currents can be used for gap filling in radar vector fields, search and rescue and oil spill response. Surface currents can also be useful to determine the origin of phytoplankton communities including potentially harmful species [26]. Moreover, HFR data can be used to derive wave characteristics [27,28]. Hourly surface currents were measured by a Coastal Ocean Dynamic Application Radar (CODAR) system; surface currents in Galway Bay are mainly driven by tide and wind forces [3,29,30]. Thus, tide and wind parameters are considered as the main input variables to develop ANN models. Mahjoobi and Adeli Mosabbeb [31] used current data and those belonging to the previous hours as inputs to predict significant wave heights using a soft computing approach (Support Vector Machine (SVM)), satisfactory forecasts were obtained. Malekmohamadi et al. [32] also used hourly wind speeds at previous time steps to predict wave heights with four different soft computing approaches—ANN, SVM, Adaptive Neuro-Fuzzy Inference System (ANFIS) and Bayesian Networks (BN). Malekmohamadi et al. [32] found that the ANN, ANFIS and SVM approaches can provide acceptable predictions for wave heights, while the BN's results are unreliable. Londhe et al. [33] used previous values of data to develop ANN models to predict forecasting errors of significant wave heights via coupling with a numerical model. Results indicate that numerical model forecasts were improved considerably by adopting an ANN approach. Gauci et al. [34] also used past measurements of HFR data and satellite wind observations to fill gaps of HFR data with ANN technique. Karimi et al. [35] used previous sea level values to establish ANN and ANFIS models. Karimi et al. [35] found that ANN and ANFIS models gave similar forecasts and outperformed auto-regression moving average models (ARMA) for all the prediction intervals. Frolov et al. [36] developed a statistical model for predicting surface currents based on historical HFR observations and forecasted winds. Frolov et al. [36] found that the minimal length of the HF-radar data required to train an accurate statistical model was between one and two years, depending on the accuracy desired. To establish an efficient short-term high accuracy forecasting system using ANN technique, the general method proposed by Mahjoobi and Adeli Mosabbeb [31] was applied in this research by taking previous observations of surface current components as input variables. The reason for including historical current data is that the variation of surface flow fields is consistent in time and space, and the development of surface flows at the present time step is significantly related to previous states. Additionally, surface currents in the Galway Bay area have significant tidal trends [37,38]. To explore and improve the forecast efficiency of ANN models, influences of the length of historical current data are investigated in details in Section 3.2. This paper also includes an intercomparison of the performance of ANN and data assimilation for short-term forecasting of surface currents to assess the merits of each approach.

The remainder of this paper is structured as follows: Section 2 presents methodologies including details of HFR system, tide and meteorological data and principles of ANN algorithm. Results are

presented in Section 3, followed by discussion in Section 4. Conclusions are finally presented in Section 5.

2. Methodologies

Forecasts of surface currents were developed using an ANN algorithm for surface currents data captured by an HFR system, tidal water elevation and meteorological data from forecasting models as input variables. Details of the approach are presented in subsequent sections.

2.1. HFR System

CODAR coastal radar systems are capable of monitoring information of surface water based on the application of high frequency radio wave backscatter [39]. Wave signals sent from radar stations in the high frequency band 3~30 MHz can receive feedback from wind-driven gravity waves of surface water when ocean waves' wavelengths are exactly half the wavelength of the broadcast radio [40–42]. Radar stations record radial surface currents; a single radar station determines the radial component of the surface currents relative to that station, providing current magnitudes and directions toward or away from that radar station. Surface flow fields are determined by synthesizing radial surface velocity components from two or more radars. The extent of alongshore surface current mapping is limited only by the number of radar systems with overlapping coverage. Spatial coverage of surface currents measured by radars can reach around 200 km, depending on transmission frequencies. Coastal radar data have applications in many areas such marine renewable energy, oil-spill monitoring [43,44], data assimilation [3,45–47], trajectory forecasts [48] and search and rescue [49].

Two radars have been deployed at Galway Bay since summer 2011 to monitor surface water movements. Radar stations are located at Mutton Island (C1 in Figure 1) and Spiddal Pier (C2 in Figure 1); the operating frequency is 25 MHz at both stations. Data from both radars are routinely transmitted to a combination center that is located in the campus of National University of Ireland, Galway. The radar system has a high spatial resolution of 300 m and maps surface flow fields every sixty minutes [50]. Measurements of surface currents from HFR system in Galway Bay have been validated with ADCP data in detail by O'Donncha et al. [29] and Ren et al. [38]. Due to environmental conditions, spatial coverage of surface flow fields varies over time. Snapshots of surface flow fields at two different times are shown in Figure 1.
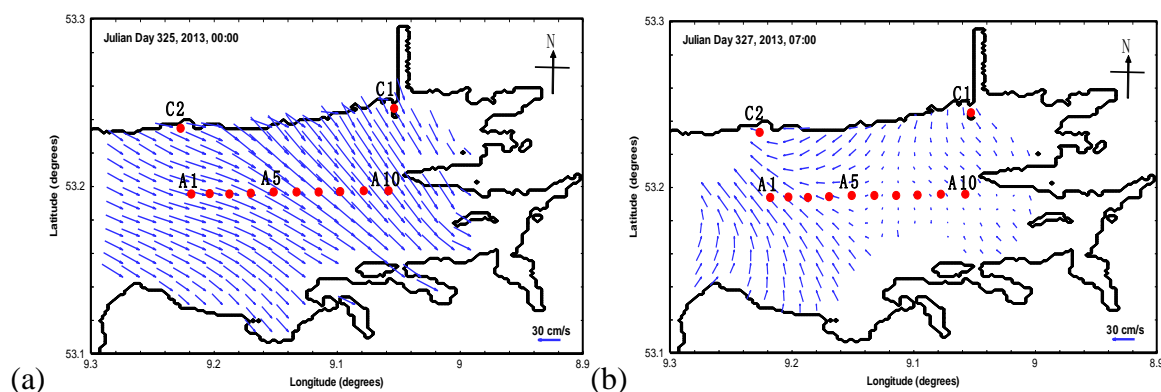
Figure 1. Deployment of CODAR system and surface flow fields of radar data: (**a**) snapshot of surface flow field at Julian Day 325, 2013, 00:00; and (**b**) snapshot of surface flow field at Julian Day 327, 2013, 07:00. A1–A10 indicate ten analysis locations and C1 and C2 denote radar stations.

Figure 1 shows that gaps of radar surface flow fields occur at certain times; this is primarily due to low surface roughness. Thus, using an efficient technique to fill observation gaps is of great importance for analyzing radar data. Lekien et al. [50] applied an improved open-boundary modal analysis (OMA) to interpolate, extrapolate and filter flows. In comparison with ANN, OMA does not depend on data.

In this research, historical data from different platforms were used to develop ANN models. One of the main tasks of this research was to establish high-accuracy short-term ANN forecast models.

Time series of surface velocity components measured by the CODAR system at ten locations (A1–A10 see Figure 1) with high coverage density from Julian Day 220 0:00 to Julian Day 365 23:00 in 2013 were selected and used to develop ANN surface current forecasting models. If east–west and north–south surface velocity components at the present time are defined as $u(t)$ and $v(t)$, respectively; and $u(t-i)$ and $v(t-i)$ indicate east–west and north–south velocity component i hour(s) before time t, respectively. Large variation existed in the magnitude and direction of surface flow vectors in the Galway Bay area. Temporal variations in surface velocity magnitudes and directions are significant and can be a big challenge when trying to simulate patterns of surface flows in Galway Bay area using numerical models. This research was concerned with investigating the capability of ANN models to predict surface velocity with such fluctuations using historical radar data and a limited number of other variables that are strongly correlated with surface currents.

2.2. Tidal Data

Water fluxes entering and exiting Galway Bay are strongly tide-induced and are primarily in the east–west direction. Tidal dynamics was one of the main driving factors used to establish ANN forecast models for Galway Bay. Tidal water elevation data obtained from Tidal Inversion Software (OTIS), developed by Oregon State University (OSU), were used in this research. The maximum range of tidal water elevation was approximately 5 m during our analysis period. The same tidal water elevation data were used for both surface velocity components at all analysis points.

2.3. Wind Data

Movement of surface water in Galway Bay is also strongly influenced by winds, especially during winter months. Wind speeds and wind directions from a meteorological forecasting model, European Centre for Medium-Range Weather Forecasts (ECMWF), were used as two other input variables to establish the ANN models. Wind data forecasts are generated by the ECMWF model every three hours. Since the overall horizontal distance between the ten analysis points (A1–A10) is approximately 20 km, two available ECMWF wind datasets (one for points A1–A5, and the other for points A6–A10) were used in our analysis. Time series of wind speeds and directions are shown in Figures 2 and 3, respectively.
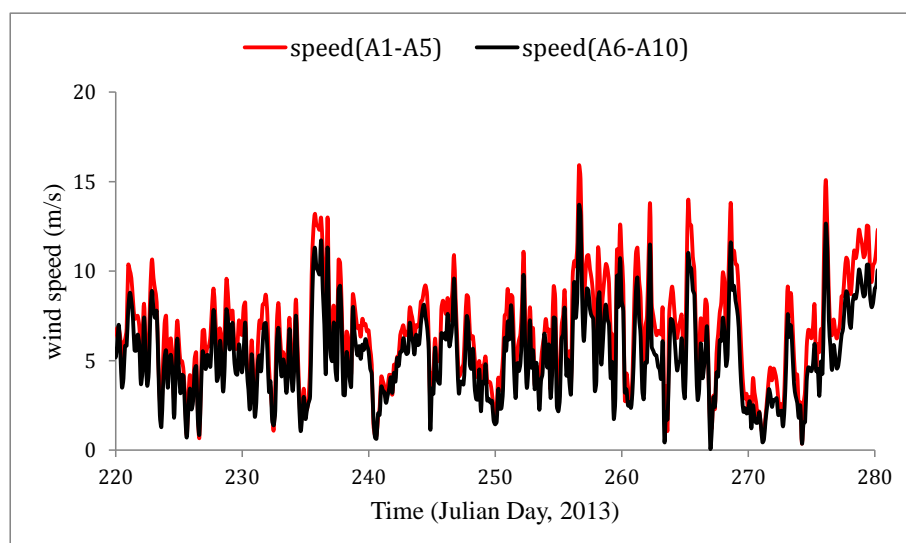
Figure 2. ECMWF wind speeds.
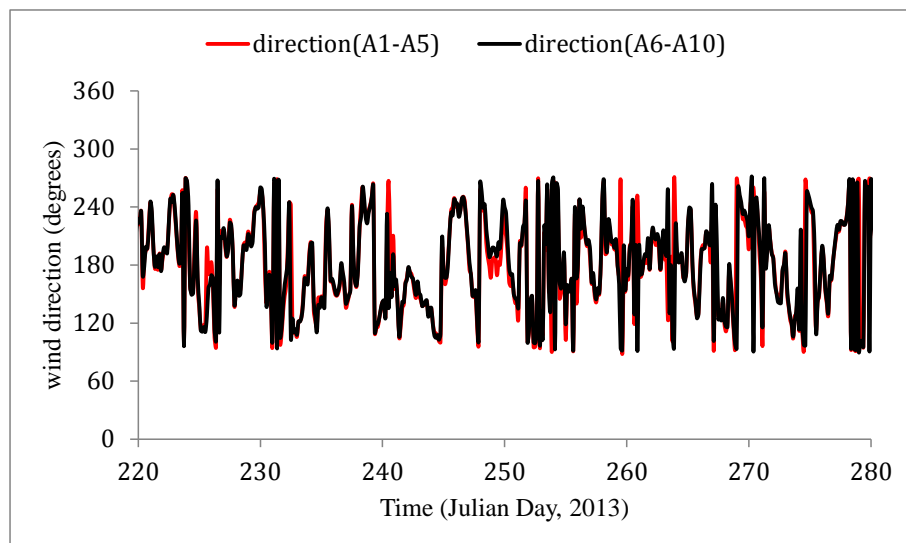
Figure 3. ECMWF wind directions.

Magnitudes of wind speeds in the domain covering points A1–A5 on average are greater than the domain including A6–A10 points in time, which may be due to the fact that points A1–A5 are located in outer Galway Bay area and so are more influenced by the Atlantic climate than points A6–A10, located in inner Galway Bay area. Averaged ECMWF wind speed for points A1–A5 is 7.17 m/s with a minimum speed 0.40 m/s and a maximum speed 19.80 m/s. Averaged ECMWF wind speed for points A6–A10 is 5.60 m/s with a minimum speed 0.20 m/s and a maximum speed 19.30 m/s. To efficiently establish ANN forecasting models for surface currents, different wind datasets from ECMWF were used for corresponding points as presented in Tables 1–3.

Table 1. Mean and range of training dataset (60% of full dataset).

Variable	Mean	Minimum	Maximum
tidal elevation (m)	0.00	−2.40	2.40
wind speed (A1–A5, m/s)	6.89	0.40	19.80
wind direction (A1–A5, degrees)	185.55	90.10	269.70
wind speed (A6–A10, m/s)	5.54	0.20	16.80
wind direction (A6–A10, degrees)	184.90	90.50	269.90
u (A1, cm/s)	−0.08	−46.80	39.30
u (A2, cm/s)	−0.02	−45.30	38.50
u (A3, cm/s)	−0.26	−44.80	38.50
u (A4, cm/s)	−0.53	−48.00	35.90
u (A5, cm/s)	−0.94	−49.70	36.10
u (A6, cm/s)	−1.45	−48.20	37.50
u (A7, cm/s)	−1.57	−48.90	40.10
u (A8, cm/s)	−2.01	−47.20	41.10
u (A9, cm/s)	−2.01	−43.70	38.70
u (A10, cm/s)	−1.55	−43.50	41.00
v (A1, cm/s)	2.04	−30.20	26.30
v (A2, cm/s)	2.64	−33.80	27.50
v (A3, cm/s)	2.93	−29.20	32.50
v (A4, cm/s)	3.05	−28.50	34.90
v (A5, cm/s)	2.97	−36.30	35.20
v (A6, cm/s)	2.46	−49.70	34.90
v (A7, cm/s)	1.23	−51.30	28.90
v (A8, cm/s)	0.66	−47.10	39.20
v (A9, cm/s)	−0.23	−38.30	24.00
v (A10, cm/s)	−1.25	−44.60	26.60

Note: u indicates surface east–west velocity component and v denotes surface north–south velocity component. Tables 2 and 3 adopt the same convention.

Table 2. Mean and range of testing dataset (20% of full dataset).

Variable	Mean	Minimum	Maximum
tidal elevation (m)	0.04	−2.20	2.10
wind speed (A1–A5, m/s)	6.51	0.40	15.80
wind direction (A1–A5, degrees)	177.81	90.30	269.60
wind speed (A6–A10, m/s)	5.19	0.50	13.40
wind direction (A6–A10, degrees)	177.33	91.70	268.50
u (A1, cm/s)	−0.91	−64.00	35.80
u (A2, cm/s)	−1.26	−60.90	36.80
u (A3, cm/s)	−1.17	−49.20	37.00
u (A4, cm/s)	−1.07	−47.30	36.70
u (A5, cm/s)	−1.64	−51.10	39.50
u (A6, cm/s)	−2.28	−51.10	41.80
u (A7, cm/s)	−3.04	−48.30	43.20
u (A8, cm/s)	−3.18	−43.70	44.20
u (A9, cm/s)	−3.00	−37.00	41.20
u (A10, cm/s)	−2.43	−39.40	37.40
v (A1, cm/s)	−3.00	−33.20	25.70
v (A2, cm/s)	−3.30	−32.90	31.40
v (A3, cm/s)	−3.10	−32.90	38.80
v (A4, cm/s)	−2.30	−36.10	40.40
v (A5, cm/s)	−1.61	−40.60	45.80
v (A6, cm/s)	−2.04	−45.80	45.60
v (A7, cm/s)	−3.11	−55.40	42.30
v (A8, cm/s)	−4.11	−46.50	28.50
v (A9, cm/s)	−3.93	−51.90	32.60
v (A10, cm/s)	−4.76	−36.60	23.20

Table 3. Mean and range of forecasting dataset (20% of full dataset).

Variable	Mean	Minimum	Maximum
tidal elevation (m)	−0.01	−2.20	2.20
wind speed (A1–A5, m/s)	8.09	0.70	19.70
wind direction (A1–A5, degrees)	188.88	90.20	269.30
wind speed (A6–A10, m/s)	6.08	0.40	19.30
wind direction (A6–A10, degrees)	188.53	90.30	269.60
u (A1, cm/s)	6.08	−38.60	49.40
u (A2, cm/s)	6.01	−36.20	44.40
u (A3, cm/s)	5.27	−36.80	44.10
u (A4, cm/s)	4.50	−36.00	46.40
u (A5, cm/s)	−3.15	−41.20	48.50
u (A6, cm/s)	1.36	−41.90	48.00
u (A7, cm/s)	1.31	−41.70	49.70
u (A8, cm/s)	1.44	−41.20	49.90
u (A9, cm/s)	0.43	−39.30	45.80
u (A10, cm/s)	1.89	−32.50	44.40
v (A1, cm/s)	5.92	−35.30	38.50
v (A2, cm/s)	6.15	−32.70	47.20
v (A3, cm/s)	4.71	−28.30	43.00
v (A4, cm/s)	4.61	−25.90	50.30
v (A5, cm/s)	5.66	−28.80	57.00
v (A6, cm/s)	6.67	−31.50	57.80
v (A7, cm/s)	5.78	−33.90	53.80
v (A8, cm/s)	4.00	−37.60	47.20
v (A9, cm/s)	3.21	−40.40	36.30
v (A10, cm/s)	2.39	−31.90	28.70

Researchers have used varying percentages of full datasets to establish ANN models to fairly and efficiently develop ANN models for short-term forecasting of surface velocity components. Datasets of tidal water elevation, wind speeds, wind directions and radar surface velocity components were divided into three categories based on the method proposed by Aydogan et al. [14]: 60% (2013 h of data) were applied to train models; 20% (670 h of data) were used for testing the models and 20% (670 h of data) were used for model forecasting. The ranges and means of each dataset are shown in Tables 1–3.

The range of surface velocity components and averaged magnitudes for the training dataset as presented in Table 1 are quite diverse for the ten locations. Similar trends exist in the testing and forecasting datasets, as presented in Tables 2 and 3. The differences in the averages and ranges of velocity components in the above three datasets are significant at the same analysis location. Diversity among training, testing and forecasting datasets can be used to examine and assess performance and robustness of the ANN models developed to generate predictions of surface velocity components at each location.

2.4. ANN Algorithm

The architecture of an ANN algorithm is generally comprised of three components [51]: a set of connections between nodes, a summation unit and a nonlinear function (see Figure 4). ANN algorithms can be used to approximate complex functional relationships between input and output variables. The ANN training process is characterized by the usage of a target output dataset that is compared to the predicted output and by adapting weights and biases based on this comparison [52]. Measurements of surface velocity components from a radar system are used as a target field to train ANN models in this research. All weights and biases are usually initialized with random magnitudes from a standard normal distribution generator [53]. A schematic of a three-layer ANN model as used in this research is shown in Figure 4.
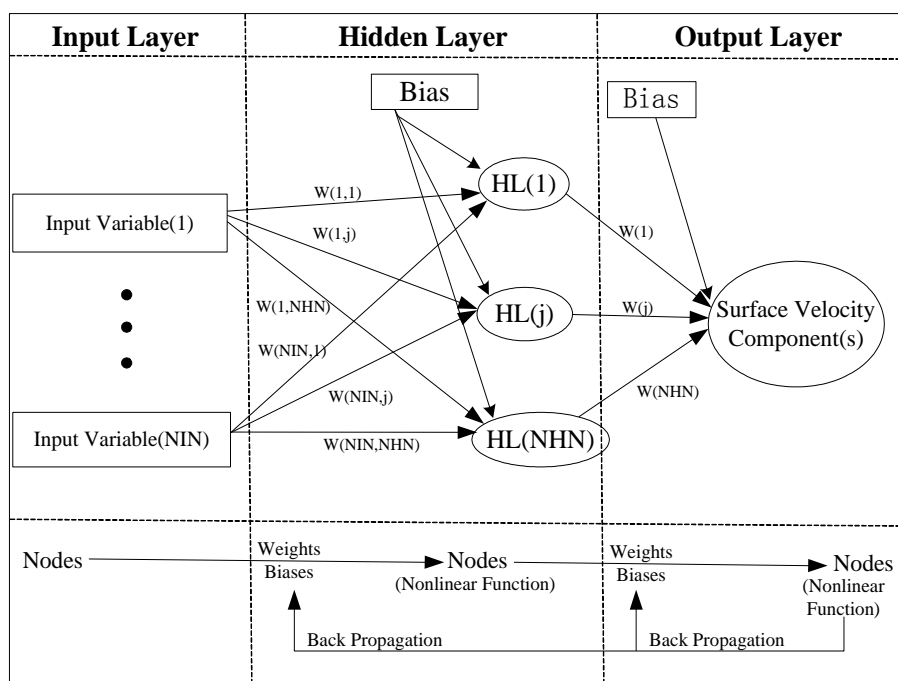
Figure 4. Schematic of a three-layer Artificial Neural Networks. w indicates weights, which varies at each connection; HL(j) indicates the *j*th node in the hidden layer; NIN indicates the total number of nodes in the input layer; and NHN indicates the total number of nodes in the hidden layer.

The weights in Figure 4 indicate the strength of the respective signals from each node. Satisfactory outputs are obtained by adjusting weights and biases of artificial nodes during the training process in comparison with the target data. As shown in Figure 4, nodes can be viewed as computational units, which receive inputs and process them to obtain outputs. Connections show the information flow between nodes. Connections can be unidirectional and bidirectional depending on the information flow [54]; connections can be a single hidden layer (HL) or multiple hidden layers. However, computational cost increases exponentially with increasing order of complexity, such as increasing the number of hidden layers [52]. Previous studies using ANN algorithm to establish forecast models suggest that a three-layer structure is capable of generating satisfactory correlations among input and output datasets [22,55,56]. Deo [1] summarized four steps to mathematically obtain outputs using ANN algorithms. Data received by nodes in the input layer are passed to nodes in the hidden layer. Each node in the hidden layer collects input information from all nodes in the input layer after multiplying each input magnitude by a weight, a bias is added and then finally the data are transformed via a nonlinear transfer function. This provides the input data for the output layer, which performs the same actions as the hidden layer. Network outputs are obtained by transforming data from each node in the output layer in a nonlinear function as presented in the Appendix A [1]. The training process of ANN models used in this research is presented in the flow chart in Figure 5.
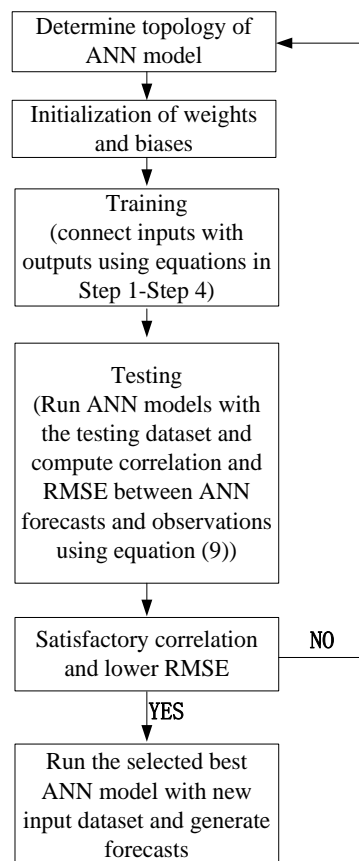
Figure 5. Flow chart of developing ANN models.

Training of an ANN model is undertaken by iteratively tuning weights and biases at each connection step for each node [57]. In this research, a flexible R package "neuralnet" was used to build the ANN models. One of the fastest algorithms, resilient back propagation, was employed due to its convergence speed, accuracy and robustness with respect to the training parameters [13,58,59]. The resilient back propagation algorithm modifies parameters of a neural network to find a local minimum of the error function [52].

3. Results

In this research, the authors focused on developing models to forecast surface currents using ANN forced with observations from radars, and tide and wind data from forecasting models. ANN forecast models for orthogonal *u* and *v* velocity components were established at ten analysis locations. The training dataset was then used to establish ANN models. The testing dataset was applied to examine and assess results from the newly developed ANN models, the best training ANN model was determined based on the model generating the minimum Room-Mean-Square-Error (RMSE) between radar observations and ANN model forecasts. The forecasting dataset was then used to make forecasts using the best ANN model.

3.1. Assessment Skills

To fairly assess performances of the ANN models, statistical values, namely correlation coefficient (R), bias, RMSE and Relative Squared Error (RSE), were computed using Equations (1)–(4) for testing the datasets. The results are presented in Tables 4 and 5 [60]. The statistical parameters are defined as:

$$\text{bias} = \overline{y} - \overline{x} \tag{1}$$

$$\text{RMSE} = \sqrt{\frac{\sum_{i=1}^{n}(y_i - x_i)^2}{n}} \tag{2}$$

$$\text{RSE} = \frac{(y_i - x_i)^2}{(\overline{x} - x_i)^2} \times 100\% \tag{3}$$

$$\text{R} = \frac{\sum_{i=1}^{n}(x_i - \overline{x})(y_i - \overline{y})}{\sqrt{\sum_{i=1}^{n}(x_i - \overline{x})^2}\sqrt{\sum_{i=1}^{n}(y_i - \overline{y})^2}} \tag{4}$$

where

x_i is an observed value;
y_i is a predicted value;
n is the number of observations; and
$\overline{x}$ and $\overline{y}$ are the means of processes x and y, respectively.

Bias indicates the trend of a measurement process to systematically over- or underestimate the value of a predicted parameter. RSE takes the total squared error between model results and observations and normalizes it by dividing the total squared error between mean of observation and actual observations; RSE is dimensionless and is expressed as a percentage. RSE is used as a measure of model accuracy. RMSE is an error index presenting an overall error distribution [61]. Correlation coefficient, R, is indicative of the linear relationship between forecasts and target values; R is particularly sensitive to outliers. Each measure has its unique usefulness as well as limitations, thus multiple statistics were evaluated to provide guidance for establishing acceptable ANN models [61].

3.2. Training and Testing

To avoid the "over-fitting problem" while training ANN models, the number of nodes in the hidden layer was determined using the formula proposed by Huang and Foo [62]:

$$\text{NHN} = 2 \times \text{NIN} + 1 \tag{5}$$

Surface current components at ten points (see Figure 1) covered by the radar system with high coverage density were separately used to develop the ANN models. The choice of appropriate input variables is most important. Tests of input variable topology were undertaken for *u* and *v* components of surface velocity, respectively. Different input structures were assessed using the testing dataset as

presented in Tables 4 and 5, the number of input variables were increased by adding longer historical observation of corresponding radar velocity component. To compare and determine appropriate input variable structures when developing ANN models, magnitudes of correlation (R), bias, RMSE and RSE were averaged at points A1–A10 for *u* and *v* velocity components, respectively, as presented in Tables 4 and 5. Model U1 only considers tidal elevation, wind speeds and directions as input variables to establish an ANN forecast model. Models U2–U12 in addition to the above three input variables also consider historical radar observations over different periods as input variables. The length of historical radar data varied from one hour $(t-1)$ to six hours $(t-6)$, corresponding to Models U2 to U12.

Table 4 shows that the ANN models for the *u* velocity component using historical velocity components as input variables can increase forecasting accuracy compared with Model U1, except for Model U5 had comparable statistics with Model U1. In general, for cases when only one historical velocity component was included (i.e., Models U2–U7), model performance deteriorated as historical data at more distant time steps were used. The averaged RMSE of the *u* velocity component at the ten locations between model results and radar measurements is relatively large in Models U1 and U5 at around 15.90 cm/s, while the averaged RMSE values are less than 10 cm/s in Models U2–U3 and U8–U12. Moreover, for these models including historical data at $(t-1)$ or $(t-2)$ were involved as input variables, high correlation (greater than 0.68) exists. Improvement of averaged RMSE at the ten analysis locations is greater than 38% (Model U3 vs. U1) for *u* velocity component in comparison with Model U1. The maximum improvement of averaged RMSE is 71% (Model U8 vs. U1) among these models. Values of RSE were less than or equal to 40% except for Model U1. The minimum value of RSE existed in Models U8, U9 and U11 (9%). This indicates that consideration of historical *u* velocity components at $(t-1)$ or $(t-2)$ in ANN models significantly improved model performance and accuracy. However, results of Models U1 and U4–U7 deviated greatly from radar observations. This illustrated that consideration of historical radar data at $(t-3)$ or more previous time steps did not have positive effects on ANN model performance.

Table 4. Averaged statistics of *u* velocity component at ten points (testing dataset).

Test	Forecasting Window (cm/s)	RMSE (cm/s)	Bias (cm/s)	R	RSE (%)
U1 (tide(t), ws(t), wd(t))	*	15.90	0.91	−0.01	102
U2 (tide(t), ws(t), wd(t), $u(t-1)$))	1	5.17	−0.04	0.94	11
U3 (tide(t), ws(t), wd(t), $u(t-2)$))	2	9.85	−0.27	0.78	40
U4 (tide(t), ws(t), wd(t), $u(t-3)$))	3	14.67	−0.07	0.39	87
U5 (tide(t), ws(t), wd(t), $u(t-4)$))	4	15.93	0.74	0.05	102
U6 (tide(t), ws(t), wd(t), $u(t-5)$))	5	15.52	1.11	0.23	97
U7 (tide(t), ws(t), wd(t), $u(t-6)$))	6	15.02	1.11	0.33	91
U8 (tide(t), ws(t), wd(t), $u(t-1)$ to $u(t-2)$))	1	4.69	0.06	0.95	9
U9 (tide(t), ws(t), wd(t), $u(t-1)$ to $u(t-3)$))	1	4.73	0.08	0.95	9
U10 (tide(t), ws(t), wd(t), $u(t-1)$ to $u(t-4)$))	1	5.45	0.2	0.94	14
U11 (tide(t), ws(t), wd(t), $u(t-1)$ to $u(t-5)$))	1	4.71	0.11	0.95	9
U12 (tide(t), ws(t), wd(t), $u(t-1)$ to $u(t-6)$))	1	5.28	0.14	0.94	13

Note: tide indicates tidal water elevation; ws and wd indicate wind speed and wind direction, respectively; $u(t-i)$ indicates east–west surface velocity component from the radar system *i* hours before the present time *t*; and * indicates that length of forecasting window varies dependent on requirements.

Models U8–U12, as presented in Table 4, were developed to examine whether combination of historical data over longer period can enhance model performance. Models U8, U9 and U11 outperformed Model U2 based on RMSE values and correlation. These results are encouraging and suggest that use of historical data over a longer period can improve model accuracy. Although performance of Models U10 and U12 was not as good as Model U2, correlations between radar data and results of these models were the same and high (0.94). In short, involving of historical data over longer period was a potential way to increase ANN model accuracy for *u* velocity component.

The same study on topology of input variables was employed for v velocity component as presented in Table 5. Model V1 considers only tidal elevation, wind speeds and directions as input variables to establish ANN forecast model. Models V2–V12 in addition to the three input variables also consider historical radar observations as input variables. The length of historical radar data varied for corresponding Models V2–V12.

Table 5. Averaged statistics of v velocity component at ten points (testing dataset).

Test	Forecasting Window (cm/s)	RMSE (cm/s)	Bias (cm/s)	R	RSE (%)
V1 (tide(t), ws(t), wd(t))	*	12.74	4.72	0.10	116
V2 (tide(t), ws(t), wd(t), $v(t-1)$)	1	5.34	0.27	0.89	20
V3 (tide(t), ws(t), wd(t), $v(t-2)$)	2	8.31	0.82	0.72	50
V4 (tide(t), ws(t), wd(t), $v(t-3)$)	3	10.45	1.55	0.50	78
V5 (tide(t), ws(t), wd(t), $v(t-4)$)	4	11.69	2.35	0.30	98
V6 (tide(t), ws(t), wd(t), $v(t-5)$)	5	12.26	2.98	0.20	108
V7 (tide(t), ws(t), wd(t), $v(t-6)$)	6	12.48	3.33	0.14	1.12
V8 (tide(t), ws(t), wd(t), $v(t-1)$ to $v(t-2)$)	1	5.12	0.48	0.90	19
V9 (tide(t), ws(t), wd(t), $v(t-1)$ to $v(t-3)$)	1	5.02	0.42	0.91	18
V10 (tide(t), ws(t), wd(t), $v(t-1)$ to $v(t-4)$)	1	5.26	0.48	0.89	20
V11 (tide(t), ws(t), wd(t), $v(t-1)$ to $v(t-5)$)	1	5.05	0.37	0.90	18
V12 (tide(t), ws(t), wd(t), $v(t-1)$ to $v(t-6)$)	1	5.48	0.33	0.89	22

Averaged statistics in Table 5 show that ANN models for the v velocity component considering historical velocity components as input variables can increase forecasting performance. When radar data at one historical time step were involved as input variables (Models V2–V7), model accuracy deteriorated as data at more distant time steps were used. Averaged RMSE values between model results and radar measurements at the ten locations is very large in Model V1 at 12.74 cm/s, while it is less in models (Models V2–V7) with data from one historical time step. Correlation between radar data and ANN model results was high (greater than 0.68) in Model V2 and V3. However, performance of Models V4–V7 was not considered good and with results approaching values achieved by Model V1. Results indicate that using historical data at $(t-1)$ or $(t-2)$ can increase model accuracy.

To further explore sensitivity of input variable structure on model performance, sensitivity models involving historical data over longer periods were examined (see Models V8–V12). Performance of Models V8–V12 was better than or comparable with the Model V2 based on RMSE values. The maximum improvement in RMSE was 61% (V9 vs. V1). Additionally, values of correlation between radar data and results in Models V8–V12 were greater than or equal to that of Model V2 (0.89). Values of RSE were less than or equal to 22% in these models. The minimum value of RSE existed in Models V9 and V11 (18%). The above analysis illustrates that consideration of historical radar data over longer periods with time steps less than $(t-5)$ positively contributed to improve model performance and accuracy. It was a potential and meaningful way to use more historical data as input variables.

The above tests for both u and v velocity components at ten locations with different structures of input variables show that the best ANN model for u and v velocity component forecasts are Models U8 and V9, respectively. Both can generate acceptably good results compared with radar data. The difference between the input variable structures of Model U8 and V9 is due to the fact that wind stresses have more influence on the v component of surface velocity than on the u component. It is seen that the addition of one extra historical data ($v(t-3)$) helped Model V9 generate better results; Model U8, forecasting the more tidally dominated u component, was able to generate satisfactory results using less historical data. It is significant to observe that the ANN approach is sensitive to dominant physical processed in such an environment.

3.3. Forecasts of Surface Velocities

To examine the performance of the best-developed ANN Models U8 and V9 with one-hour forecasting lead-time, the predicted surface current components at location A3 and A8 (see Figure 1) are shown in Figures 6–9.
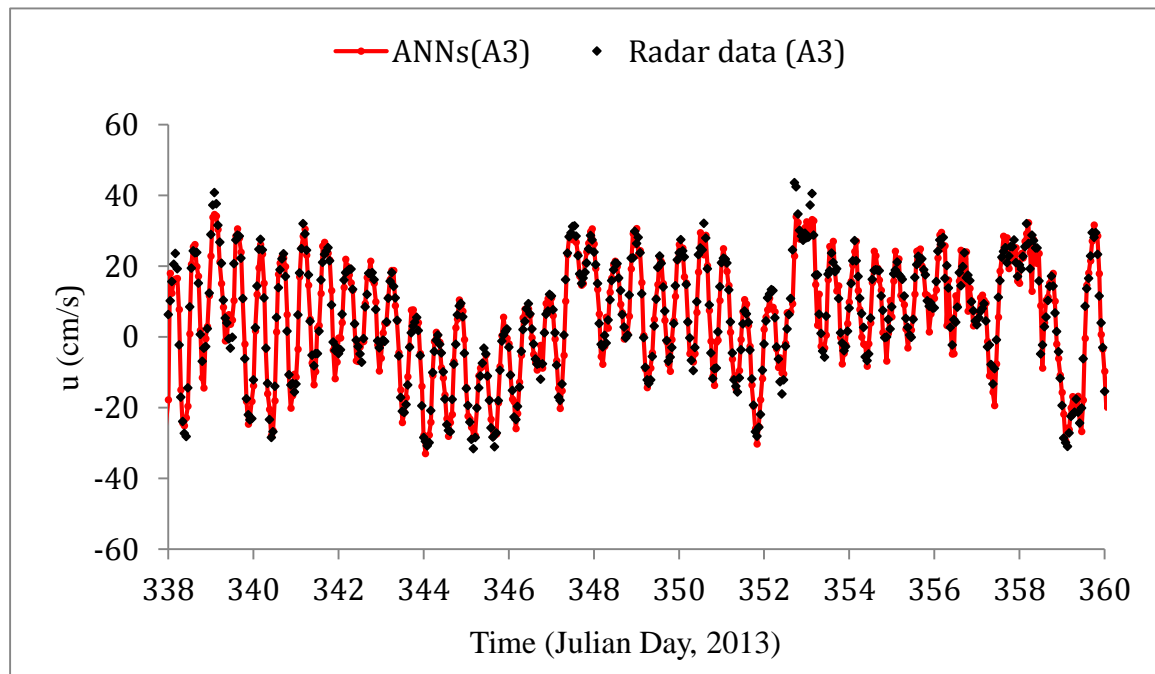
Figure 6. Forecasts of *u* velocity component at A3 (Model U8, 1 h forecast window).
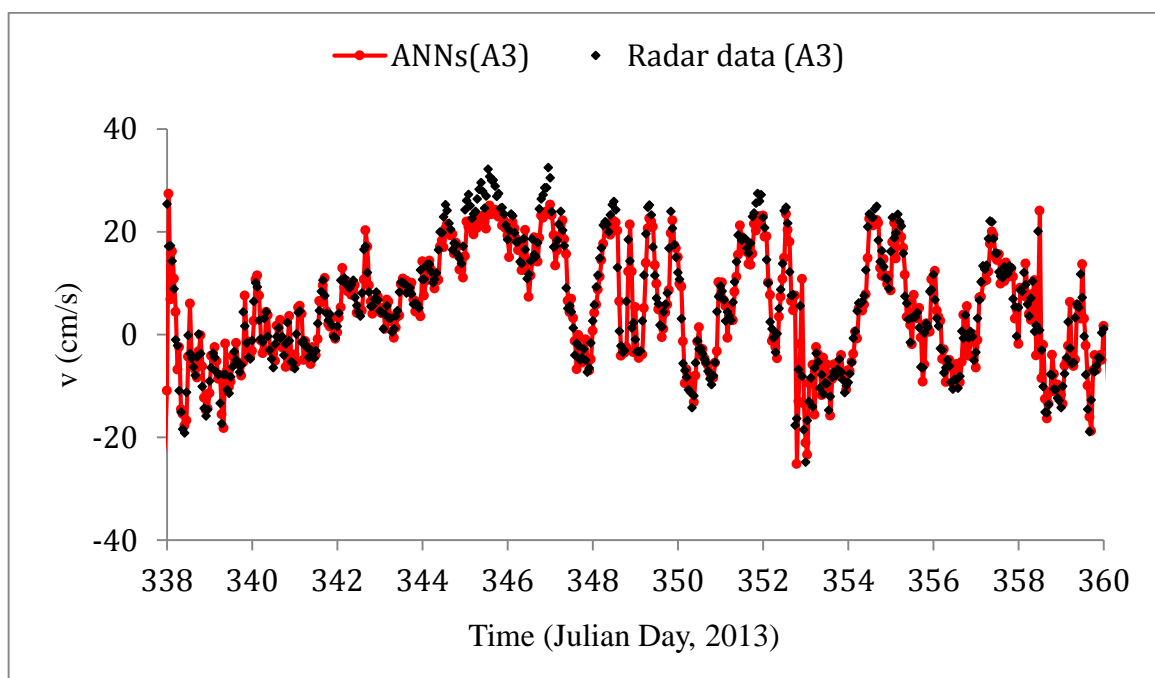
Figure 7. Forecasts of *v* velocity component at A3 (Model V9, 1 h forecast window).
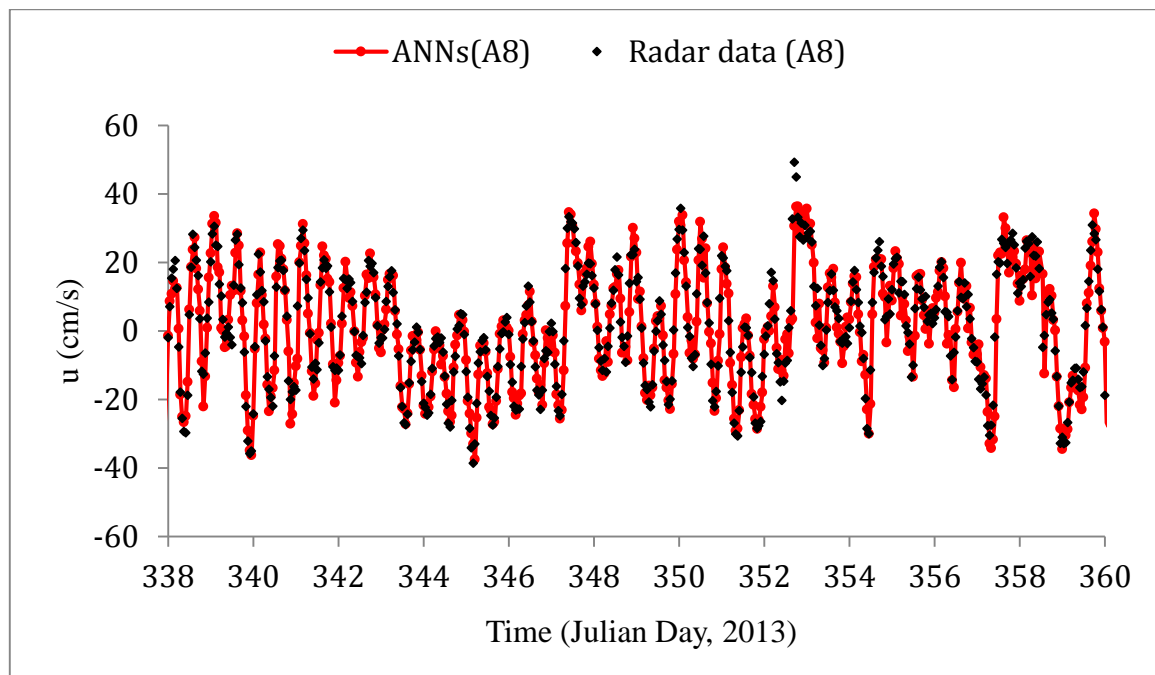
Figure 8. Forecasts of *u* velocity component at A8 (Model U8, 1 h forecast window).
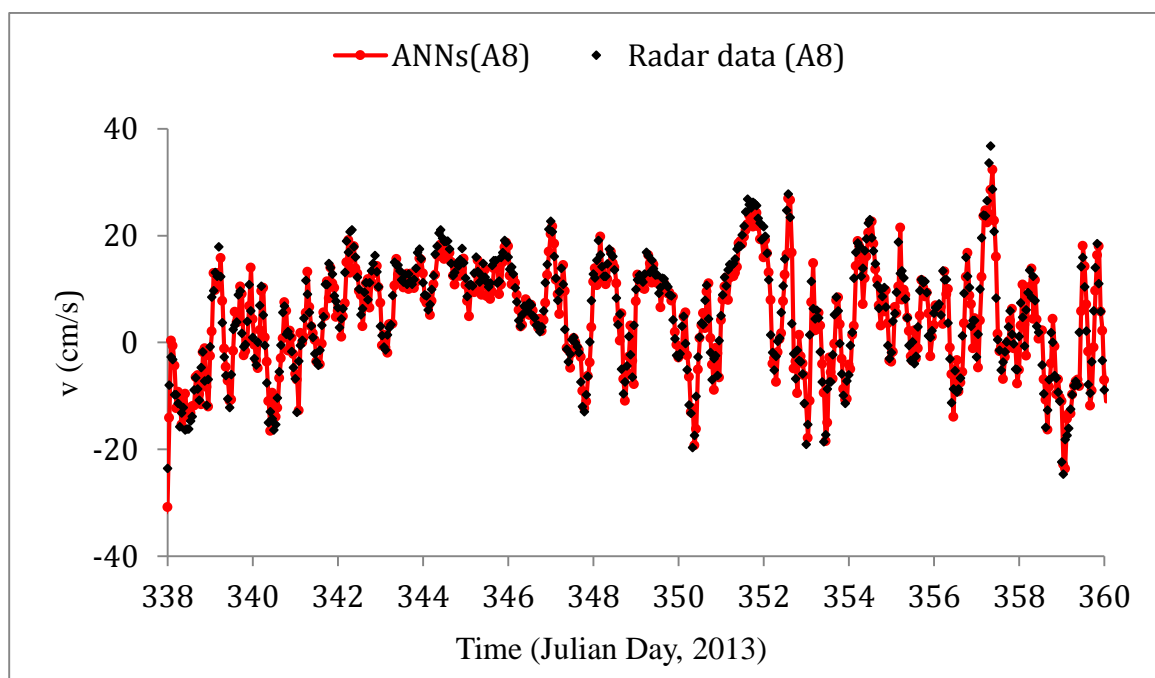
Figure 9. Forecasts of *v* velocity component at A8 (Model V9, 1 h forecast window).

Figures 6 and 7 show that Models U8 and V9 can produce good agreement for corresponding east–west and north–south velocity components in comparison with radar data over a long forecast period (approximately 28 days) at location A3 with a one-hour forecasting lead time. Significant deviation exists only at a few time steps, such as Julian Days 352–354 for *u* velocity component (see Figure 6) and Julian Days 345–347 for *v* velocity component (see Figure 7). Correlation coefficients for both surface velocity components between predicted results and radar data at location A3 are greater than 0.92.

Figures 8 and 9 show that Models U8 and V9 can produce forecast of both surface velocity components having high correlation with radar data over a long forecast period at location A8 with one-hour forecasting lead-time as well. Again, significant deviation exists at only a few time steps, such as Julian Days 352–354 for *u* velocity component and Julian Days 352–353 for *v* velocity component. Correlation coefficients for both surface velocity components between predicted results and radar data at location A8 are greater than 0.93.

To quantitatively assess model forecasts at each of the output locations within Galway Bay, values of RMSE, bias, correlation coefficient (R) and RSE of forecasts from ANN models using the forecast dataset for 670 h at each location are computed using Equations (1)–(4) and presented in Tables 6 and 7.

Table 6 shows that the range of RMSE between forecasts of *u* velocity component from Model U8 and radar data at ten locations is 4.29–5.15 cm/s. Additionally, the range of *u* velocity components at ten points is −41.9–49.9 cm/s, as presented in Table 3. RMSE between ANN forecasts and radar data was less than 5% of the *u* velocity component range on average. Correlation coefficient is equal to or greater than 0.95 at all locations. This indicates that Model U8 using tidal elevation forecast, wind speeds and directions, and historical *u* velocity components at previous two hours as input variables is capable of yielding satisfactory forecasts in domain.

Table 6. Statistics of *u* velocity component forecasts (Model U8, 1 h forecast window).

Point	RMSE (cm/s)	Bias (cm/s)	R	RSE (%)
A1	5.15	−0.43	0.96	8
A2	4.29	−0.48	0.97	8
A3	4.71	−0.40	0.96	8
A4	4.34	−0.37	0.97	6
A5	4.45	−0.28	0.97	6
A6	4.70	−0.38	0.96	7
A7	4.90	−0.17	0.96	7
A8	5.04	−0.25	0.96	8
A9	4.61	−0.24	0.96	9
A10	4.59	−0.39	0.95	11

Table 7 shows that the range of RMSE values of *v* velocity component between results from Model V9 and radar data at ten locations is 3.69–5.66 cm/s. Moreover, the range of *v* velocity components at the points is −40.4 to 57.8 cm/s, as presented in Table 3. RMSE between ANN forecasts and radar data was less than 5% of the *v* velocity component range on average. Correlation coefficients are equal to or greater than 0.90 at all locations. This indicates that Model V9 with input variables including tidal elevation forecast, wind speeds and directions, and historical *v* velocity components at previous three hours has an ability to generate good forecasts in the domain.

Table 7. Statistics of *v* velocity component forecasts (Model V9, 1 h forecast window).

Point	RMSE (cm/s)	Bias (cm/s)	R	RSE (%)
A1	4.14	−0.79	0.94	12
A2	4.43	−0.83	0.94	13
A3	4.99	−0.50	0.92	15
A4	4.79	−0.30	0.93	14
A5	5.20	−0.44	0.92	16
A6	5.66	−0.78	0.90	20
A7	5.38	−0.77	0.90	20
A8	4.36	−0.43	0.93	13
A9	4.41	−0.69	0.91	18
A10	3.69	−0.28	0.94	12

Forecasts of *u* velocity components from Model U8 have higher correlations with radar data (Table 6) than for *v* velocity component from Model V9 (Table 7) at all analysis locations. The range of

the RMSE values of v velocity components is greater than for the u velocity components. Absolute values of bias in v velocity components are greater than u velocity components. This suggests that more significant satisfactory forecasts of east–west flows can be produced by Model U8 than north–south flows by Model V9. This may be because tide-induced flows in the east–west in direction are more deterministic than the strongly wind dominated north–south flows which are more random in nature. Generally, values of RSE for u velocity components at the ten analysis points were smaller than those of the v velocity component. Again, this indicates that Model U8 produced more accurate predictions than Model V9.

The forecasting window of the ANN Models U8 and V9 is one hour. However, a longer forecasting window is desirable for various practical applications such as search and rescue and oil spill response. To examine the influence of adopting historical data as input variables on ANN model performance and to extend forecast window, experiments on forecasting windows for both surface velocity components at the ten analysis locations were performed in the following section.

3.4. Forecasting Window Tests

To generate satisfactory forecasts over a longer forecasting window, tidal elevation, wind speeds and directions at different historical time steps were used as input variables in additional test Models U13–U19 and V13–V19, as presented in Tables 8 and 9. Since Galway Bay hydrodynamics are affected by semi-diurnal periodic tides [37], radar data of velocity components, wind speed and direction 12 h before the prediction time t were also examined as input variables to assess sensitivity of results in Models U17–U19 and V17–V19. Input variable structures and averaged values of RMSE, bias, R and RSE using the testing dataset are computed using Equations (1)–(4) and are presented in Tables 8 and 9 corresponding to the u and v velocity, respectively.

Table 8. Averaged statistics of u velocity component at ten locations (testing dataset).

Test	Forecasting Window (cm/s)	RMSE (cm/s)	Bias (cm/s)	R	RSE (%)
U13 (tide(t), ws(t), wd(t), $u(t-2)$, $u(t-3)$)	2	8.04	0.11	0.86	27
U14 (tide(t), ws(t), wd(t), $u(t-3)$, $u(t-4)$)	3	10.58	0.12	0.75	46
U15 (tide(t), ws(t), wd(t), $u(t-4)$, $u(t-5)$)	4	13.01	0.33	0.60	69
U16 (tide(t), ws(t), wd(t), $u(t-5)$, $u(t-6)$)	5	14.98	0.83	0.38	91
U17 (tide(t), ws(t), wd(t), $u(t-3)$, $u(t-4)$, $u(t-12)$)	3	10.05	0.29	0.77	42
U18 (tide(t), ws(t), wd(t), $u(t-3)$, $u(t-4)$, $u(t-12)$, ws($t-12$))	3	10.14	0.25	0.77	42
U19 (tide(t), ws(t), wd(t), $u(t-3)$, $u(t-4)$, $u(t-12)$, ws($t-12$), wd($t-12$))	3	10.61	0.27	0.75	46

Table 9. Averaged statistics of v velocity component at ten locations (testing dataset).

Test	Forecasting Window (cm/s)	RMSE (cm/s)	Bias (cm/s)	R	RSE (%)
V13 (tide(t), ws(t), wd(t), $v(t-2)$, $v(t-3)$, $v(t-4)$)	2	7.91	1.03	0.75	45
V14 (tide(t), ws(t), wd(t), $v(t-3)$, $v(t-4)$, $v(t-5)$)	3	11.56	1.86	0.54	111
V15 (tide(t), ws(t), wd(t), $v(t-4)$, $v(t-5)$, $v(t-6)$)	4	11.29	2.20	0.39	91
V16 (tide(t), ws(t), wd(t), $v(t-5)$, $v(t-6)$, $v(t-7)$)	5	12.12	2.68	0.23	106
V17 (tide(t), ws(t), wd(t), $v(t-2)$, $v(t-3)$, $v(t-4)$, $v(t-12)$)	3	7.93	0.84	0.75	45
V18 (tide(t), ws(t), wd(t), $v(t-2)$, $v(t-3)$, $v(t-4)$, $v(t-12)$, ws($t-12$)	3	7.91	0.83	0.75	45
V19 (tide(t), ws(t), wd(t), $v(t-2)$, $v(t-3)$, $v(t-4)$, $v(t-12)$, ws($t-12$), wd($t-12$))	3	8.69	0.50	0.69	55

Tables 8 and 9 show averaged values of RMSE between radar data and ANN model forecasts at the ten analysis locations. In general, values of RMSE increase as the forecasting window becomes longer; and correlation between radar data and predicted results deteriorate significantly as the forecasting window becomes longer (U13–U16 and V13–V16). This is because auto-correlations among u components of surface currents are stronger when the lag is smaller. Based on a correlation assessment system, as proposed by Taylor [63], high correlation (greater than 0.68) exists in Models U13, U14 and V13. This indicates that Model U14 using historical data ($u(t-3)$, $u(t-4)$) is capable

of producing satisfactory forecasts for the *u* velocity component. Values of RMSE between testing dataset (20% of the full dataset) and radar data as presented in Table 8 increase significantly from Model U13 to Model U16. Model V13 using historical data ($v(t-2)$, $v(t-3)$, $v(t-4)$) can yield satisfactory forecasts for *v* component of surface velocity. Model U14 with a three-hour forecasting window and Model V13 with a two-hour forecasting window can generate closer results to HFR data with high correlation (≥ 0.75). RMSE values in Models U13, U14 and V13 were better or comparable with Eulerian RMSE value (9 cm/s) in the first 6 h forecasts obtained by Frolov et al. [36]. To compare and evaluate forecasts, forecasts of surface velocity components are compared with radar data at the location A3. as shown in Figures 10 and 11 respectively.
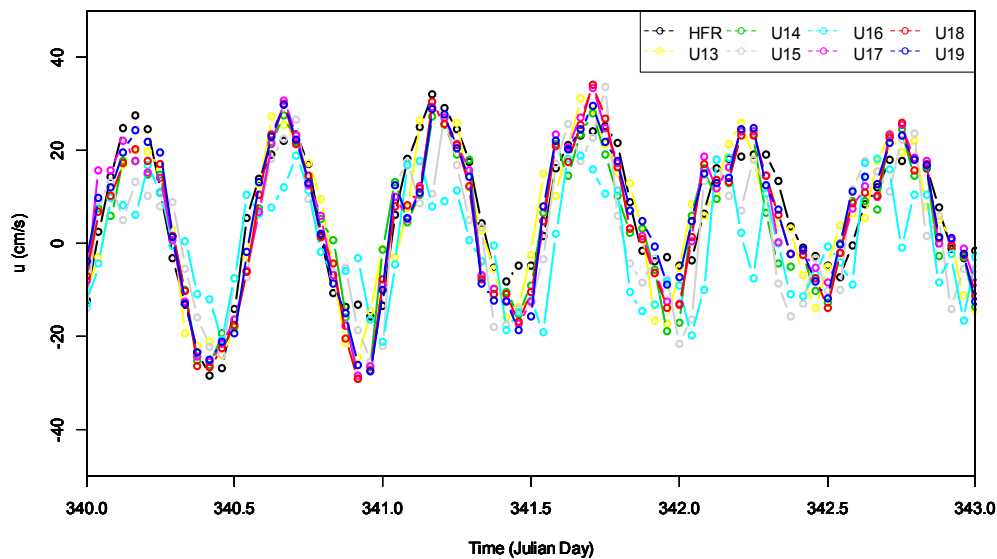
Figure 10. Forecasts of *u* velocity component at A3.
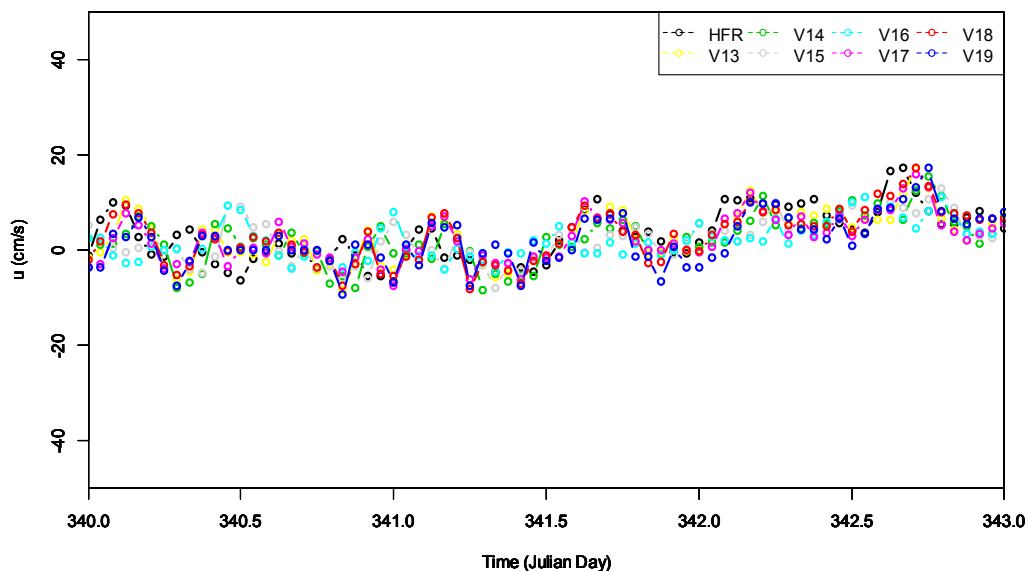
Figure 11. Forecasts of *v* velocity component at A3.

Based on the good performance of Models U14 and V13, Models U17–U19 and V17–V19 as presented in Tables 8 and 9 were used to assess model accuracy through considering tidal elevation, historical HFR data, wind speed and wind direction 12 h before forecasting time t as input variables. Statistics in Table 8 illustrate that Models U17 and U18, using tidal elevation or wind speed 12 h prior,

slightly enhance model performance for *u* velocity components in comparison with U9. Improvement of RMSE for *u* velocity component in Model U17 is 5% relative to Model U14. Table 9 shows that the addition of velocity component and wind speed 12 h before time t slightly affects model performance (see Model V13 vs. Model V18); however, when wind direction at the previous 12 h is included, model performance deteriorates (see Model V18 vs. Model V19). This may be because variations in wind direction occur quickly. It is observed that by including wind direction 12 h before forecast time does not have a strong positive influence on surface current forecasts. The best forecasting ANN models having a relatively long forecasting window are Models U17 and V18, as shown in Figures 10 and 11. Additionally, the value of RSE in Model V19 was significantly increased when including wind direction 12 h before the forecasting time.

In general, good agreement exists between the radar data and forecasts from Model V18. Averaged correlation coefficient of *u* velocity component between radar data and ANN predictions at the ten analysis points using the same input structure as Model U17 is greater than 0.8, the value of averaged correlation coefficient at the ten analysis points is greater than 0.77 for *v* velocity component using the same input structure as Model V18.

The authors previously developed hydrodynamic models of Galway Bay and used data assimilation (DA) to assimilate radar data into the model to improve model results; these models were then used to generate forecasts of surface currents. Ren and Hartnett [5] and Ren et al. [3] used Optimal Interpolation data assimilation algorithm and assimilation of indirect correction of wind stress. Here, we compare the forecasts obtained using the simpler ANN models to forecasts using DA models. Models U17 and V18 were used to produce prediction of surface velocity components at A3 during the same forecasting period as the best data assimilation models from Ren and Hartnett [5] and Ren et al. [3]. Time series of prediction for both surface velocity components are shown in Figures 12 and 13.
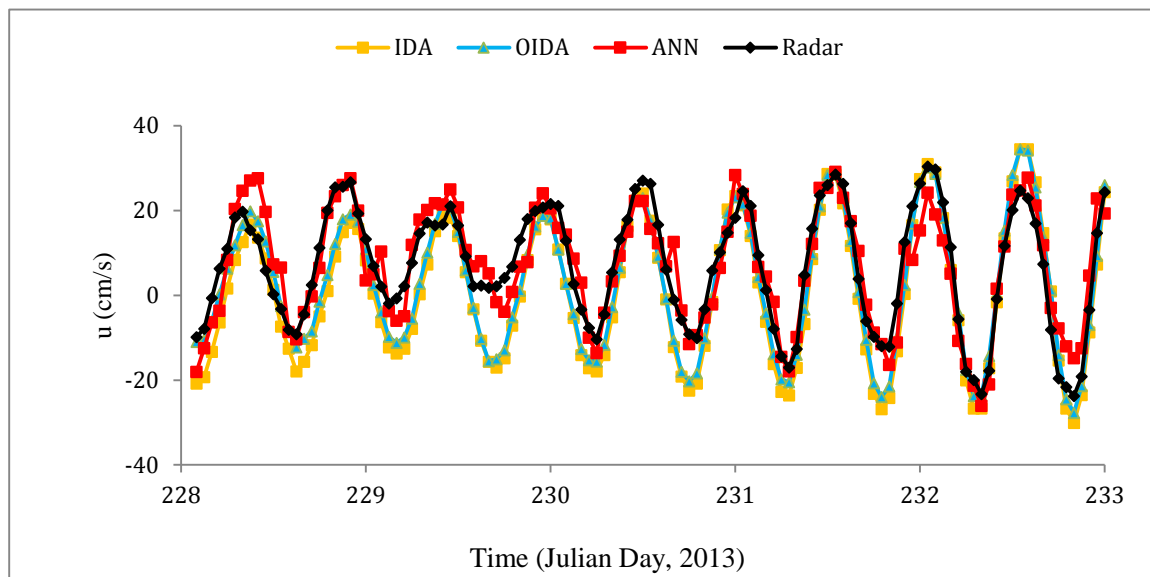
Figure 12. Forecasting of east–west velocity component at A3. IDA and OIDA indicate data assimilation using Optimal Interpolation and indirect correction method, respectively, the same convention of IDA and OIDA was used as follows. ANN indicates Model U17.
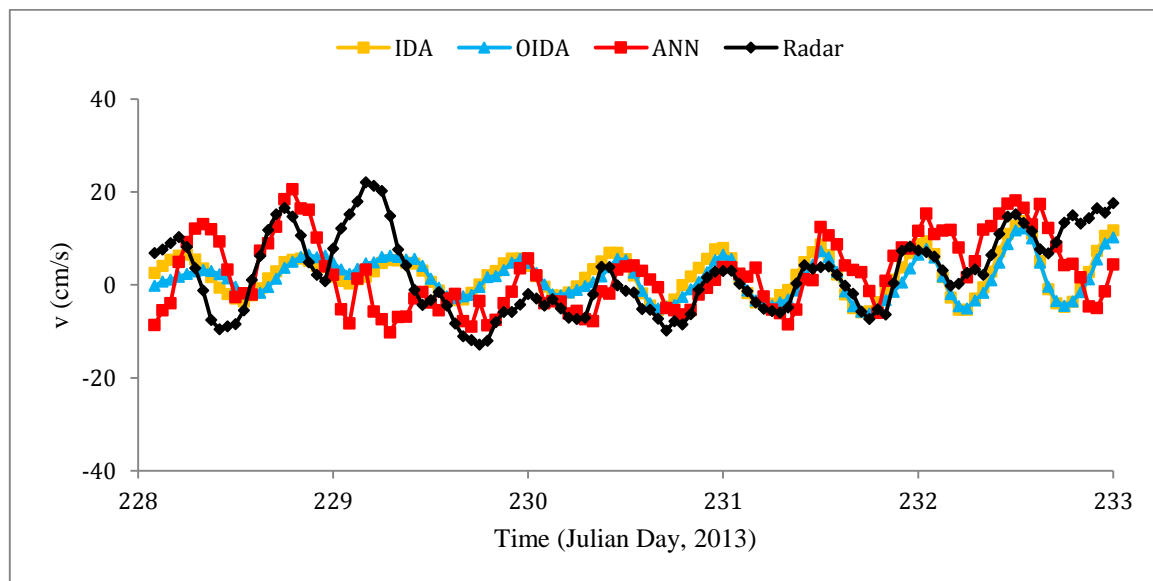
Figure 13. Forecasting of north–south velocity component at A3. ANN indicates results of the Model V18.

Figure 12 illustrates that ANN Model U17 generally outperformed data assimilation models using Optimal Interpolation and indirectly correction of wind stress. Better performance from ANN models is significant at peak times of surface east–west velocity component. RMSE values between model results and radar data during the five-day period are presented in Table 10.

Table 10. RMSE between HFR data and model results (A3, cm/s).

Variable	ANN	OIDA	IDA
u	5.69	7.27	8.90
v	6.39	7.23	7.22

Note that calculation period is from Julian day 228–233, 2013.

Table 10 shows that ANN Model V18 produces consistently better predictions than the data assimilation models. Improvement in RMSE for u and v velocity component is 36% and 11%, respectively, relative to the IDA model results, and 22% and 12%, respectively, relative to the OIDA model results. Moreover, the computational costs of the ANN model were significantly lower than data assimilation models; this is very attractive for forecasting systems.

4. Discussion

The ANN models developed for both surface velocity components using tidal water elevation, wind speeds and direction, and historical radar surface currents are capable of generating short-term forecasts of surface currents with high accuracy during a 3-h forecasting window. Significant aspects of this research are: historical radar data were applied to produce forecasts of surface currents using ANN algorithm at a range of locations over a large domain; the input variable structure was assessed by analyzing the results of a range of input variables; the practical forecasting window of surface velocity components was extended by choosing "older" historical radar data; and performance of predictions was evaluated in comparison with radar data over a relatively long period. The ANN forecast models could be used for activities such as gap filling of radar data, oil spill response and search and rescue. The short-term forecasts developed herein are more accurate than attempts made by previous research efforts. Correlation coefficients of u velocity component between ANN forecasts and

radar data over 670 h were greater than 0.95 at all analysis points, as presented in Table 6. Correlation coefficients of *v* velocity component were greater than 0.90 as presented in Table 7. These correlation values were greater than those (0.76–0.79) produced by Mathew and Deo [64] using ANN, Decision Tree and nonlinear regression to predict wind speeds.

Saha et al. [61] also used ANN to generate forecasts of surface currents using results from a hybrid coordinate ocean model (HYCOM) and oceanographic buoy observations. The use of a model as input to the ANN forecasts is a significant difference from the approach adopted by the authors; the authors' approach is an attractive alternative since it does not rely on computational requirements and hence is more efficient.

RMSE values of surface *u* and *v* velocity components between the model forecasts and observations over different lead time obtained by Saha et al. [61] were in the order of 15.89 cm/s and 15.21 cm/s, respectively, which are generally larger than the averaged RMSE values obtained in this research at ten location over a wide range using Models U17 and V18 for surface *u* and *v* components separately by 10.05 cm/s and 7.91 cm/s. As lead-time became longer, RMSE values in their study increased. Correlation coefficients of *u* velocity component between model predictions and observations obtained by Saha et al. [61] ranging from 0.82 to 0.93 are stronger than the value in this research from Model U17 (0.77); however, Model V18 in this research had a stronger correlation coefficient (0.75) for velocity *v* component than those correlation coefficients when the lead time was greater than three days in the study by Saha et al. [61]. This is particularly encouraging since the authors' forecast did not use a detailed numerical model as input.

Furthermore, according to the RMSE between ANN model results and observations, forecasts of surface currents produced in this research were significantly better than vertical currents at depths generated by Aydogan et al. [14], in which RMSE was greater than 10 cm/s and 16 cm/s on average for *u* and *v* velocity components, respectively. In addition, the correlation coefficient of velocity *u* component (0.95) between results from Model U8 and HFR data was better than that value (0.93) obtained by Gauci et al. [34] for radar data gap filling; however, their correlation coefficient (0.93) was slightly better than that value (0.91) for velocity *v* component between results from Model V9 and HFR data. Thus, the accuracy achieved by the authors when forecasting is of the same order obtained by others in gap filling (in effect hindcasting), which is an easier process using data available at the time of interest rather than forecasting.

This is the first time that research has been developed using ANN to extend forecasting windows using historical HFR data. Comparative studies presented in Tables 8 and 9 show that using HFR data $u(t-3)$, $u(t-4)$, $u(t-12)$ and $v(t-2)$, $v(t-3)$, $v(t-4)$, $v(t-12)$ as input variables within ANN models produce satisfactory forecasts for *u* and *v* velocity components, respectively.

5. Conclusions

In this research, an ANN technique was employed to establish predictive models for surface currents in Galway Bay. Tidal elevations, radar data wind speeds and directions were chosen as input variables for an ANN predictive model. Based on previous studies, and to further extend model forecast ability, surface velocity components from radars at previous observation time steps were used as input variables and tested. *u* and *v* components of surface velocities were the output variables of the ANN models. The results indicate that an ANN approach can produce satisfactory correlations for both surface velocity components. ANN models can generate high-accuracy forecasts of both surface velocity components over short term durations. The main conclusions from this research are:

(a) Incorporating historical radar measurements as input variables can produce high accuracy forecasts with a one-hour forecasting window. Correlation coefficients between predicted results and HFR data are greater than or equal to 0.95 for *u* velocity components. Correlation coefficients are greater than or equal to 0.90 for *v* velocity components. Using the above objective measures, these forecasts represent very high degrees of accuracy [63].

(b)   Very strong correlations (equal to or greater than 0.90) and small RMSE values at ten locations for both *u* and *v* components of surface currents show that ANN algorithms can be used as a powerful tool to predict surface currents with one-hour forecasting window at single/multiple points or over a domain. Thus, forecasts of surface flow fields throughout a domain can be obtained when historical radar observations are available. This can also be used for filling radar observation gaps due to variation in environmental conditions, which has significant implications for analysis and presentation of coastal radar data.

(c)   A models are capable of producing satisfactory forecasts over a three-hour forecasting window for *u* component of surface velocity. As expected, correlation coefficients decrease with increasing forecasting window. Strong correlations (i.e., 0.75 greater than 0.68 for significance proposed by Taylor [63]) are achieved when the forecasting window is equal to or less than three hours. Satisfactory forecasts of *v* component of surface velocity can be obtained from ANN models when a forecasting window is equal to or less than two hours. Correlation of *v* velocity component between observations and model results has a negative trend as the forecasting window increases.

(d)   RMSE values and a skill score assessment show that ANN models outperformed complex, computationally expensive data assimilation models using: (i) optimal interpolation; and (ii) indirect correction of wind stress.

(e)   Once an ANN model has been established and verified, forecasts can be efficiently generated for a wide range of environmental forcing conditions. ANN algorithms provide a promising approach for the development of forecasting models due to computational efficiency, ease of implementation and accuracy.

Results indicate that ANN models can generate short-term accurate forecasts for surface velocity components. Such forecasting has many real world applications such as hindcasting/reanalysis; providing accurate and real-time information for search and rescue and oil spill response; generating forecasts of currents at marine renewable turbine test site; and hydro-environmental monitoring. Since spatial coverage of the radar surface vector fields varies over time, ANN models can be adopted to accurately fill measurement gaps in time and space. In summary, the application of HFR data within ANN algorithms under appropriate considerations provides a very useful approach to generate forecasts of surface velocity components. It is important that the structure of input variables is carefully examined when ANN model is used to forecast surface currents in other domains.

In future research, the authors are interested in using numerical model results as ANN inputs when HFR data are not available to develop hybrid ANN models.

Author Contributions: L.R. conceived and ran models; and L.R., Z.H. and M.H. wrote this paper.

Conflicts of Interest: The authors declare no conflict of interest.

Appendix A. ANN Algorithm

Generally, steps of ANN algorithm can be summarized as follows [1]:

Step 1: Sum up weighted inputs

$$S_j^{input} = \sum_{i=1}^{NIN} (w_{ij}^{ANN} x_i^{ANN}) + \beta_j \tag{A1}$$

where

S_j^{input} is the summation of the *j*th node in the hidden layer, $j = 1, 2, \ldots, NHN$;

NIN is the total number of nodes in the input layer;

w_{ij}^{ANN} is the connection weight between the *i*th node in the input layer and the *j*th node in the hidden layer, $i = 1, 2, \ldots, NIN$;

x_i^{ANN} is the input at the *i*th node in the input layer; and

β_j is the bias at the *j*th node in the hidden layer.

Step 2: Transform the weighted input

$$O_j^{HL} = f\left(S_j^{input}\right) \tag{A2}$$

where

O_j^{HL} is the output from the *j*th node in the hidden layer; and

$f(\cdot)$ is an activation function.

Step 3: Sum up the node outputs in the hidden layer

$$S_k^{output} = \sum_{j=1}^{NHN}\left(w_{jk}^{ANN}O_j^{HL}\right) + \theta_k \tag{A3}$$

where

S_k^{output} is the summation of the *k*th node in the output layer ($k \geq 1$);

NHN is the total number of nodes in the hidden layer;

w_{jk}^{ANN} is the connection weight between the *j*th node in the hidden layer and *k*th node in the output layer; and

θ_k is the bias at the *k*th node in the output layer.

Step 4: Transform the weighted sum

$$O_k^{output} = f\left(S_k^{output}\right) \tag{A4}$$

where

O_k^{output} is the *k*th node output in the output layer.

The objective of the ANN algorithm is to reduce the global squared error E_{ANN} in the following formula:

$$E_{ANN} = \frac{1}{P_{train}}\sum_{i=1}^{P_{train}} E_{P_{train}} \tag{A5}$$

$$E_{P_{train}} = \frac{1}{2}\sum_{k=1}^{NOUT}\left(O_k^{output} - O_k^{target}\right)^2 \tag{A6}$$

where

P_{train} is the total number of training patterns;

$NOUT$ is the total number of nodes in the output layer;

O_k^{target} is the target output at the *k*th node in the output layer;

E_{ANN} is the global squared error; and

$E_{P_{train}}$ is the squared error at the *p*th training pattern.

The best training models are built up by generating an acceptable global squared error E_{ANN}. To reduce the global squared error, each of the weights and biases in the network were updated during the back propagation procedure [65]. Firstly, the partial derivative of the global squared error with respect to the tuning weight was computed. Secondly, adding the product of the computed partial derivative and learning rate from the original weight obtained new weight. This procedure was repeated until a satisfactory global squared error was obtained [57,66].

The functions in Step 2 and Step 4 are called transfer or activation functions. There are various options for the functions used in these steps such as linear activation functions, sigmoid activation

functions and Gaussian activation functions. Sibi et al. [67] analyzed the impacts of different activation functions using back propagation neural networks and concluded that there is not a huge difference in performance using different activation functions when a network was trained up successfully. In this research, a sigmoid activation function was adopted to establish ANN models under consideration of the nonlinear relationships among input and output variables [68]:

$$f(x) = \frac{1}{1 + e^{-x}} \tag{A7}$$

The same transfer Equation (1) was used in Step 2 and Step 4 in this research.

References

1. Deo, M.C. Artificial neural networks in coastal and ocean engineering. *Indian J. Geo-Mar. Sci.* **2010**, *39*, 589–596.
2. Moore, A.M.; Arango, H.G.; Broquet, G.; Powell, B.S.; Weaver, A.T.; Zavala-Garay, J. The Regional Ocean Modeling System (ROMS) 4-dimensional variational data assimilation systems: Part I—System overview and formulation. *Prog. Oceanogr.* **2011**, *91*, 34–49. [CrossRef]
3. Ren, L.; Nash, S.; Hartnett, M. Forecasting of Surface Currents via Correcting Wind Stress with Assimilation of High-Frequency Radar Data in a Three-Dimensional Model. *Adv. Meteorol.* **2016**, *2016*, 1–12. [CrossRef]
4. Ren, L.; Hartnett, M. Prediction of surface currents using High Frequency CODAR data and Decision Tree at a marine renewable test site. In Proceedings of the 3rd International Conference on Energy and Environmental Research, Barcelona, Spain, 7–11 September 2016.
5. Ren, L.; Hartnett, M. Sensitivity analysis of a data assimilation technique for hindcasting and forecasting hydrodynamics of a complex coastal water body. *Comput. Geosci.* **2016**, *99*, 81–90. [CrossRef]
6. He, Z.; Wen, X.; Liu, H.; Du, J. A comparative study of artificial neural network, adaptive neuro fuzzy inference system and support vector machine for forecasting river flow in the semiarid mountain region. *J. Hydrol.* **2014**, *509*, 379–386. [CrossRef]
7. Mekanik, F.; Imteaz, M.A.; Talei, A. Seasonal rainfall forecasting by adaptive network-based fuzzy inference system (ANFIS) using large scale climate signals. *Clim. Dyn.* **2015**, *46*, 3097–3111. [CrossRef]
8. Timofeev, R. Classification and Regression Trees (CART) Theory and Applications. Master's Thesis, Humboldt University, Berlin, Germany, 2004.
9. Vilibic, I.; Sepic, J.; Mihanovic, H.; Kalinic, H.; Cosoli, S.; Janekovic, I.; Zagar, N.; Jesenko, B.; Tudor, M.; Dadic, V.; et al. Self-Organizing Maps-based ocean currents forecasting system. *Sci. Rep.* **2016**, *6*, 22924. [CrossRef] [PubMed]
10. Mau, J.-C.; Wang, D.-P.; Ullman, D.S.; Codiga, D.L. Characterizing Long Island Sound outflows from HF radar using self-organizing maps. *Estuar. Coast. Shelf Sci.* **2007**, *74*, 155–165. [CrossRef]
11. Liu, Y.; Weisberg, R.H. Patterns of ocean current variability on the West Florida Shelf using the self-organizing map. *J. Geophys. Res.* **2005**, *110*, 1–12. [CrossRef]
12. Wang, Y.; Ma, X.; Joyce, M.J. Reducing sensor complexity for monitoring wind turbine performance using principal component analysis. *Renew. Energy* **2016**, *97*, 444–456. [CrossRef]
13. Chen, C.S.; Lin, J.M. Applying Rprop neural network for the prediction of the mobile station location. *Sensors* **2011**, *11*, 4207–4230. [CrossRef] [PubMed]
14. Aydogan, B.; Ayat, B.; Öztürk, M.N.; Özkan Çevik, E.; Yüksel, Y. Current velocity forecasting in straits with artificial neural networks, a case study: Strait of Istanbul. *Ocean Eng.* **2010**, *37*, 443–453. [CrossRef]
15. Partal, T.; Cigizoglu, H.K.; Kahya, E. Daily precipitation predictions using three different wavelet neural network algorithms by meteorological data. *Stoch. Environ. Res. Risk Assess.* **2015**, *29*, 1317–1329. [CrossRef]
16. Makarynskyy, O.; Pires-Silva, A.A.; Makarynska, D.; Ventura-Soares, C. Artificial neural networks in wave predictions at the west coast of Portugal. *Comput. Geosci.* **2005**, *31*, 415–424. [CrossRef]
17. Yang, W.; Xia, X. Prediction of mining subsidence under thin bedrocks and thick unconsolidated layers based on field measurement and artificial neural networks. *Comput. Geosci.* **2013**, *52*, 199–203. [CrossRef]
18. Erzin, Y.; Cetin, T. The prediction of the critical factor of safety of homogeneous finite slopes using neural networks and multiple regressions. *Comput. Geosci.* **2013**, *51*, 305–313. [CrossRef]
19. Zabada, S.; Shahrour, I. Analysis of Heating Expenses in a Large Social Housing Stock Using Artificial Neural Networks. *Energies* **2017**, *10*, 2086. [CrossRef]

20. Makarynsky, O.; Makarynska, D. Wave Prediction and Data Supplementation and Artificial Neural Networks. *J. Coast. Res.* **2007**, *23*, 951–960. [CrossRef]

21. Sztobryn, M. Forecast of storm surge by means of artificial neural network. *J. Sea Res.* **2003**, *49*, 317–322. [CrossRef]

22. Makarynskyy, O. Improving wave predictions with artificial neural networks. *Ocean Eng.* **2004**, *31*, 709–724. [CrossRef]

23. Zhang, Z.; Li, C.-W.; Qi, Y.; Li, Y.-S. Incorporation of artificial neural networks and data assimilation techniques into a third generation wind wave model for wave forecasting. *J. Hydroinform.* **2006**, *8*, 65–76. [CrossRef]

24. Huang, W.; Murray, C. Multiple-station neural network for modelling tidal currents across Shinnecock inlet, USA. *Hydrol. Process.* **2008**, *22*, 1136–1149. [CrossRef]

25. Krasnopolsky, V.M.; Chalikov, D.V.; Tolman, H.L. A neural network technique to improve computational efficiency of numerical oceanic models. *Ocean Model.* **2002**, *4*, 363–383. [CrossRef]

26. Cianelli, D.; D'Alelio, D.; Uttieri, M.; Sarno, D.; Zingone, A.; Zambianchi, E.; d'Alcalà, M.R. Disentangling physical and biological drivers of phytoplankton dynamics in a coastal system. *Sci. Rep.* **2017**, *7*, 1–15. [CrossRef] [PubMed]

27. Atan, R.; Goggins, J.; Hartnett, M.; Agostinho, P.; Nash, S. Assessment of wave characteristics and resource variability at a 1/4-scale wave energy test site in Galway Bay using waverider and high frequency radar (CODAR) data. *Ocean Eng.* **2016**, *117*, 272–291. [CrossRef]

28. Lorente, P.; Sotillo, M.G.; Aouf, L.; Amo-Baladrón, A.; Barrera, E.; Dalphinet, A.; Toledano, C.; Rainaud, R.; Alfonso, M.D.; Piedracoba, S.; et al. Extreme Wave Height Events in NW Spain: A Combined Multi-Sensor and Model Approach. *Remote Sens.* **2018**, *10*, 1. [CrossRef]

29. O'Donncha, F.; Hartnett, M.; Nash, S.; Ren, L.; Ragnoli, E. Characterizing observed circulation patterns within a bay using HF radar and numerical model simulations. *J. Mar. Syst.* **2014**, *142*, 96–110. [CrossRef]

30. Dabrowski, T. A Flushing Study Analysis of Selected Irish Waterbodies. Ph.D. Thesis, National University of Ireland Galway, Galway, Ireland, 2005.

31. Mahjoobi, J.; Adeli Mosabbeb, E. Prediction of significant wave height using regressive support vector machines. *Ocean Eng.* **2009**, *36*, 339–347. [CrossRef]

32. Malekmohamadi, I.; Bazargan-Lari, M.R.; Derachian, R.; Nikoo, M.R.; Fallahnia, M. Evaluating the efficacy of SVMs, BNs, ANNs and ANFIS in wave height prediction. *Ocean Eng.* **2011**, *38*, 487–497. [CrossRef]

33. Londhe, S.N.; Shah, S.; Dixit, P.R.; Nair, T.M.B.; Sirisha, P.; Jain, R. A coupled numerical and artificial neural network model for improving location specific wave forecast. *Appl. Ocean Res.* **2016**, *59*, 483–491. [CrossRef]

34. Gauci, A.; Drago, A.; Abela, J. Gap Filling of the CALYPSO HF Radar Sea Surface Current Data through Past Measurements and Satellite Wind Observations. *Int. J. Navig. Obs.* **2016**, *2016*, 1–9. [CrossRef]

35. Karimi, S.; Kisi, O.; Shiri, J.; Makarynskyy, O. Neuro-fuzzy and neural network techniques for forecasting sea level in Darwin Harbor, Australia. *Comput. Geosci.* **2013**, *52*, 50–59. [CrossRef]

36. Frolov, S.; Paduan, J.; Cook, M.; Bellingham, J. Improved statistical prediction of surface currents based on historic HF-radar observations. *Ocean Dyn.* **2012**, *62*, 1111–1122. [CrossRef]

37. Wen, L. Three-Dimensional Hydrodynamic Modelling in Galway Bay. Ph.D. Thesis, University College Galway, Galway, Ireland, 1995.

38. Ren, L.; Nash, S.; Hartnett, M. Observation and modeling of tide- and wind-induced surface currents in Galway Bay. *Water Sci. Eng.* **2015**, *8*, 345–352. [CrossRef]

39. Paduan, J.D.; Washburn, L. High-Frequency Radar Observations of Ocean Surface Currents. *Ann. Rev. Mar. Sci.* **2013**, *5*, 115–136. [CrossRef] [PubMed]

40. Lipa, B.J.; Barrick, D.E.; Isaacson, J.; Lilieboe, P.M. CODAR Wave Measurements From a North Sea Semisubmersible. *IEEE J. Ocean. Eng.* **1990**, *15*, 119–125. [CrossRef]

41. Emery, B.M.; Washburn, L.; Harlan, J.A. Evaluating radial current measurements from CODAR High-Frequency radars with moored current meters. *J. Atmos. Ocean. Technol.* **2004**, *21*, 1259–1271. [CrossRef]

42. Liu, Y.; Weisberg, R.H.; Merz, C.R.; Lichtenwalner, S.; Kirkpatrick, G.J. HF Radar Performance in a Low-Energy Environment: CODAR SeaSonde Experience on the West Florida Shelf. *J. Atmos. Ocean. Technol.* **2010**, *27*, 1689–1710. [CrossRef]

43. Tinis, S.W.; Hodgins, D.O.; Fingas, M. Assimilation of Radar Measured Surface Current Fields into a Numerical Model for Oil Spill Modelling. *Spill Sci. Technol. Bull.* **1996**, *3*, 247–251. [CrossRef]

44. Bellomo, L.; Griffa, A.; Cosoli, S.; Falco, P.; Gerin, R.; Iermano, I.; Kalampokis, A.; Kokkini, Z.; Magaldi, M.G.; Mamoutos, I.; et al. Toward an integrated HF radar network in the Mediterranean Sea to improve search and rescue and oil spill response: The TOSCA project experience. *J. Oper. Oceanogr.* **2015**, *8*, 95–107. [CrossRef]

45. Marmain, J.; Molcard, A.; Forget, P.; Barth, A.; Ourmières, Y. Assimilation of HF radar surface currents to optimize forcing in the northwestern Mediterranean Sea. *Nonlinear Process. Geophys.* **2014**, *21*, 659–675. [CrossRef]

46. Xu, J.; Huang, J.; Gao, S.; Cao, Y. Assimilation of high frequency radar data into a shelf sea circulation model. *J. Ocean Univ. China* **2014**, *13*, 572–578. [CrossRef]

47. Ren, L.; Nash, S.; Hartnett, M. Renewable Energies Offshore. In *Chapter 24 Data Assimilation with High-Frequency (HF) Radar Surface Currents at a Marine Renewable Energy Test Site*; Soares, C.G., Ed.; CRC Press: London, UK, 2015.

48. Solabarrieta, L.; Frolov, S.; Cook, M.; Paduan, J.; Rubio, A.; González, M.; Mader, J.; Charria, G. Skill Assessment of HF Radar-Derived Products for Lagrangian Simulations in the Bay of Biscay. *J. Atmos. Ocean. Technol.* **2016**, *33*, 2585–2597. [CrossRef]

49. Roarty, H.; Glenn, S.; Allen, A. Evaluation of Environmental Data For Search and Rescue. In Proceedings of the OCEANS 2016, Shanghai, China, 10–13 April 2016; pp. 1–3.

50. Lekien, F.; Coulliette, C.; Bank, R.; Marsden, J. Open-boundary modal analysis: Interpolation, extrapolation, and filtering. *J. Geophys. Res.* **2004**, *109*. [CrossRef]

51. Ai, N.; Wu, Z.; Ren, J. Support Vector Machine and Artificial Neural Network. *J. Shandong Univ. Technol. (Sci. Tech.)* **2005**, *19*, 45–49.

52. Giinther, F.; Fritsch, S. neuralnet: Training of Neural Networks. *R J.* **2010**, *2*, 421–430.

53. Jain, A.K.; Mao, J.; Mohiuddin, K.M. Artificial Neural Networks: A tutorial. *Computer* **1996**, *29*, 31–44. [CrossRef]

54. Gershenson, C. Artificial Neural Networks for Beginners. *arXiv* **2003**.

55. Tsai, C.P.; Lin, C.; Shen, J.N. Neural network for wave forecasting among multi-stations. *Ocean Eng.* **2002**, *29*, 1683–1695. [CrossRef]

56. Deo, M.C.; Jha, A.; Chaphekar, A.S.; Ravikant, K. Neural networks for wave forecasting. *Ocean Eng.* **2001**, *28*, 889–898. [CrossRef]

57. Yegnanarayana, B. *Artificial Neural Networks*; Prentice-Hall of India Private Limited: Delhi, India, 2006.

58. Almeida, C.; Baugh, C.M.; Lacey, C.G.; Frenk, C.S.; Granato, G.L.; Silva, L.; Bressan, A. Modelling the dusty universe—I. Introducing the artificial neural network and first applications to luminosity and colour distributions. *Mon. Not. R. Astron. Soc.* **2010**, *402*, 544–564. [CrossRef]

59. Kumar, A.; Zhang, D. Personal recognition using hand shape and texture. *IEEE Trans. Image Process.* **2006**, *15*, 2454–2461. [CrossRef] [PubMed]

60. Mahjoobi, J.; Etemad-Shahidi, A. An alternative approach for the prediction of significant wave heights based on classification and regression trees. *Appl. Ocean Res.* **2008**, *30*, 172–177. [CrossRef]

61. Saha, D.; Deo, M.C.; Joseph, S.; Bhargava, K. A combined numerical and neural technique for short term prediction of ocean currents in the Indian Ocean. *Environ. Syst. Res.* **2016**, *4*, 1–14. [CrossRef]

62. Huang, W.; Foo, S. Neural network modeling of salinity variation in Apalachicola River. *Water Res.* **2002**, *36*, 356–362. [CrossRef]

63. Taylor, T. Interpretation of the Correlation Coefficient: A Basic Review. *J. Diagn. Med. Sonogr.* **1990**, *6*, 35–39. [CrossRef]

64. Mathew, T.E.; Deo, M.C. Inverse estimation of wind from the waves measured by high-frequency radar. *Int. J. Remote Sens.* **2012**, *33*, 2985–3003. [CrossRef]

65. Deo, M.C.; Naidu, C.S. Real time wave forecasting using neural networks. *Ocean Eng.* **1998**, *26*, 191–203. [CrossRef]

66. Larsen, J. Introduction to Artificial Neural Networks. Available online: http://www2.imm.dtu.dk/pubdb/views/edoc_download.php/2443/pdf/ (accessed on 25 May 2018).

67. Sibi, P.; Jones, S.A.; Siddarth, P. Analysis of different activation functions using back propgation neural networks. *J. Theor. Appl. Inf. Technol.* **2013**, *47*, 1264–1268.

68. Jain, P.; Deo, M.C. Real-time wave forecasts off the western Indian coast. *Appl. Ocean Res.* **2007**, *29*, 72–79. [CrossRef]